

# Effect of Niobium on Phase Transformations, Mechanical Properties and Corrosion of Supermartensitic Stainless Steel

Mariana Perez de Oliveira, José Wilmar Calderón-Hernández, Rodrigo Magnabosco, Duberney Hincapie-Ladino, and Neusa Alonso-Falleiros

(Submitted July 20, 2016; in revised form December 30, 2016; published online March 17, 2017)

The influence of niobium addition in a supermartensitic stainless steel with 13Cr-5Ni-2Mo has been studied. The steel with Nb tempered at 600 °C for 2 h showed improved mechanical resistance properties and lower degree of sensitization, without compromising elongation and pitting corrosion resistance, when compared to the reference steel. In order to understand the Nb effect in such steel, mainly regarding phase transformation, different tempering time intervals have been studied. The better performance of the SM2MoNb is attributed to the hindering effect that Nb has in the kinetics of the phase transformations during tempering, delaying the precipitation start and coarsening stages of the present phases.

**Keywords** mechanical properties, niobium, pitting corrosion, sensitization, supermartensitic stainless steel, tempering

## 1. Introduction

The constant increase in oil and gas demand has made reserves, previously not considered economically feasible, to become viable sources of energy. However, such reserves demand specific project solutions, considering their unique features. One family of materials that is being used as a solution to moderate H<sub>2</sub>S and CO<sub>2</sub> effects is the supermartensitic stainless steel, which can contain 13 to 16%Cr and up to 5%Mo for improved corrosion resistance (Ref 1).

As supermartensitic stainless steels (SMSS) have low interstitial levels ( $C + N < 0.10\%$ ) and contain Cr and Mo, additions of Ni (up to 7%) are used to guarantee that the solubilization happens completely at the gamma loop and, therefore, that martensite forms upon quenching (Ref 1).

In order to obtain a good compromise between mechanical resistance and toughness, tempering treatment is always necessary after quenching. Tempering is usually performed at temperatures between 500 and 700 °C (Ref 2, 3).

After tempering, the final microstructure consists of a tempered martensite matrix, essentially a body-centered cubic—BCC—structure. In that matrix, other phases can be found. Retained austenite after quenching is usual, and during tempering austenite suffers coalescence, since it is an equilibrium phase at usual tempering temperatures. Finely dispersed

precipitates are also found, and they can be Chi phase and/or carbides; however, carbides are found in very low fractions due to small amounts of carbon found in SMSS. The proportion between such phases will depend not only on the chemical composition of the steel, but also on the temperature and duration of the applied heat treatment (Ref 3).

During tempering and welding of this type of steels, even at such low carbon and nitrogen levels, the precipitation of chromium carbide could occur in a wide range of temperatures (400–800 °C) (Ref 4). This could prejudice the steel corrosion resistance as a whole and, if it occurs at the grain boundaries, which is frequently the case, the steel becomes sensitized. To avoid sensitization, stabilizing elements such as niobium and titanium could be added to the steel in order to avoid chromium carbide precipitation, which can frequently be the cause of a lower corrosion performance of the material (Ref 1, 5–9). Besides improving corrosion resistance, such alloying elements can also increase mechanical properties through secondary hardening during tempering (Ref 6, 8).

Niobium additions in supermartensitic stainless steels have been studied only recently and by few authors (Ref 6–10). Zou et al. (Ref 10) have evaluated the influence of tempering temperature (520 a 720 °C) and time (3–12 h) in the mechanical properties of a supermartensitic stainless steel containing 12.5%Cr, 4.38%Ni, 0.96%Mo, 0.02%Nb and 0.1%V, with  $C + N$  levels below 0.07%. It was concluded that the best compromise between yield strength, tensile strength, elongation and hardness is obtained after 3 h tempering at 600 °C, condition where austenite content is estimated at 13 vol.%. The authors also reported the occurrence of secondary hardening, observed due to an increase in hardness between 520 and 680 °C, attributed to the formation of both carbides during tempering and of non-tempered martensite during cooling.

A series of papers have been published about higher niobium additions in supermartensitic stainless steels (Ref 6–9). One of the studies (Ref 6) focused on two chemical compositions (13Cr5Ni1Mo-0.01N and 13Cr5Ni1Mo-0.01N-0.1Nb) and in six tempering temperatures (550, 575, 600, 625, 650 or 700 °C). Quenching was performed after solution treatment at 1050 °C for 30 min. The authors stated that the addition of

Mariana Perez de Oliveira, Companhia Brasileira de Metalurgia e Mineração (CBMM), Araxá, Brazil; José Wilmar Calderón-Hernández, Duberney Hincapie-Ladino, and Neusa Alonso-Falleiros, Department of Metallurgical and Materials Engineering, Polytechnic School, University of São Paulo, São Paulo, Brazil; and Rodrigo Magnabosco, Department of Materials Engineering, FEI University, São Bernardo do Campo, Brazil. Contact e-mail: wilmarcalderon100@gmail.com.

0.1%Nb in low interstitial 13%Cr-5%Ni-1%Mo decreases the amount of Cr-rich precipitates, as Nb combines preferentially with carbon and nitrogen, forming nanoprecipitates. Such precipitates, besides being beneficial to avoid sensitization, are also responsible to enhanced strength. After tempering at 600 °C for 2 h, the steel with Nb exhibited yield strength 30% higher than the reference steel, with enough elongation (close to 20%) and Charpy toughness (160 J at room temperature). The authors have also concluded that Nb retards the kinetics of austenite formation during tempering, which was called reversed austenite by the authors.

Compositions with double the Mo content (2%) were also investigated seeking better corrosion resistance (Ref 8). The samples were submitted to the same heat treatment in previous studies: solution treatment at 1050 °C for 30 minutes followed by air cooling and tempering for 2 h at temperatures between 550 and 700 °C. The highest mechanical properties have been achieved by the composition containing Nb (13Cr5Ni2Mo-0.1Nb0.01N) in the tempering temperatures varying from 550 to 625 °C. Tempering temperature of 600 °C was chosen for the best compromise between mechanical resistance, toughness and elongation. Pitting corrosion resistance was evaluated in this tempering condition at 3.5%NaCl aerated solution: the best pitting corrosion resistance was obtained for the steel with 2%Mo and Nb addition (0.11%).

The present work studies the influence of niobium addition in the mechanical and corrosion resistance properties of a 13Cr-5Ni-2Mo supermartensitic stainless steel tempered at 600 °C for different time periods, focusing on the phase transformation aspects. It presents a detailed analysis of the microstructure evolution, and a deeper understanding on how phases formed during tempering affect mechanical properties and corrosion resistance.

## 2. Materials and Experimental Procedures

Two supermartensitic stainless steels have been studied: SM2Mo and SM2MoNb. As it can be observed in Table 1, the steels present similar chemical composition, being Nb addition the main difference.

Steels samples were melted and processed in laboratory scale elsewhere (Ref 6-9) and have been received in the form of hot rolled plates, with 10 mm thickness. They have been submitted to annealing at 1050 °C for 48 h, in order to eliminate the presence of delta-ferrite (Ref 11), followed by quenching in oil. This has been followed by another heat treatment step for adjustment of grain size; samples have been heated at 1050 °C for 30 minutes followed by quenching in oil. Tempering was then performed at 600 °C for different time periods (1, 2, 4 or 8 h). Samples in the as-quenched condition have also been included in the study, identified as 0 h condition.

Thermodynamic equilibrium calculations using ThermoCalc software (version 3.1, TCFE7 database) were performed in

order to predict possible phases present at 600 °C. Microstructural characterization has been performed in embedded samples, after etching with Vilella, through scanning electron microscope (SEM—FEI INSPECT F50). X-ray diffraction (XRD) using Cu-K $\alpha$  radiation has been used to detect present phases (Shimadzu, XRD-7000), and the volume fraction of non-magnetic phases was measured in all samples with a Feritscope (Helmut-Fischer, MP30). Mechanical strength was determined by HRC hardness measurements—performed according ASTM E18-14 (Ref 12) for all the samples in all conditions. Tensile tests according ASTM A370:2010—sections 5 to 13 (Ref 13)—were performed in three samples of each steel in the 2 h tempering condition only, since this is considered the regular tempering time used by the industry.

Corrosion resistance tests for determination of the degree of sensitization (DOS) and pitting potential were performed in a PAR 273A potentiostat. Tests were conducted in an electrochemical cell containing a platinum counter electrode and saturated calomel as the reference electrode. For the determination of DOS, a scanning rate of 1.67 mV/s (6V/h) was used, while for defining the pitting potential, the scanning rate used was 1 mV/s. After all tests, samples have been analyzed by optical microscope (OM) and scanning electron microscope (SEM).

DOS was determined for both steels in all the conditions by the DL-EPR method (double loop electrochemical potentiokinetic reactivation technique) in 1M H<sub>2</sub>SO<sub>4</sub> + 0.01M KSCN electrolyte. The resulting DL-EPR curves showed two maximum current peaks: the activation current density ( $i_a$ ) and reactivation current density ( $i_r$ ). Degree of sensitization (DOS), or the sensitization level, was determined as the percent ratio  $i_r/i_a$ .

Pitting corrosion resistance has been determined for both steels in the 2 h tempering condition through cyclic anodic polarization curves in 3.5% NaCl aqueous solution, naturally aerated. Pitting potential ( $E_p$ ), or the potential where nucleation and continued growth of at least one pit is possible, was determined as the potential where there is an inclination shift in the electrode potential versus current density curve.

## 3. Results

### 3.1 Characterization of the Industrial Condition: 2 h Tempering at 600 °C

Results for the tensile tests of both steels at 600 °C and 2 h tempering are shown in Table 2. SM2MoNb steel shows 18% higher yield strength and tensile strength average values when compared to SM2Mo. According with ISO 13680:2010 (Ref 14), both steels could be classified as Grade 110. However, it is important to point out that SM2MoNb steel is in the standard upper limit, indicating the possibility of obtaining a higher seamless pipe grade, not specified in the standard. The same standard also establishes 32 HRC as the maximum average hardness for 13-5-2 (0,02%C, 13%Cr, 5%Ni, 2%Mo), Grade

**Table 1 Chemical composition of SM2Mo and SM2MoNb steels (wt.%)**

Steel	C	N	Si	Mn	P	S	Cr	Ni	Mo	Nb	Ti
SM2Mo	0.020	0.013	0.42	0.51	0.016	0.004	12.59	5.01	1.90	...	0.0062
SM2MoNb	0.022	0.010	0.41	0.48	0.016	0.006	12.91	5.16	2.05	0.11	0.0043

110 steel. Both steels are in accordance with the standard as both of them showed HRC hardness values of  $29 \pm 3$ .

Regarding pitting corrosion resistance, both steels have also presented similar behavior, as shown by the curves in Fig. 1 and by  $E_p$  average values in Table 3: both steels can be considered as having the same pitting corrosion resistance for the conditions studied.

Typical DL-EPR curves for both steels are presented in Fig. 2. As shown in Table 4, the steel with Nb was less prone to suffer sensitization than the SM2Mo steel due to the difference in the DOS obtained: the SM2Mo steel has double the DOS than the steel with Nb, and this is confirmed by the optical microscopy exam of the samples after DL-EPR curves, shown in Fig. 3. SM2Mo steel has a more etched microstructure than the steel with Nb, which means that the SM2Mo steel has a higher Cr-depleted area fraction. Such Cr-depleted regions are originated around chromium-rich phases probably formed during tempering.

SEM analysis of 2 h-tempered samples of both steels after DL-EPR tests are presented in Fig. 4. It can be observed that both steels present phases precipitated within the martensite packages with similar morphology, with a higher amount of precipitated phases in the SM2Mo steel (Fig. 4a) when compared to the steel with Nb addition (Fig. 4b). According to the optical microscope of the samples after the DOS tests, probably the phases presented in the steel SM2Mo are chromium-rich phases. This, however, could not be confirmed by EDS analysis due to the nanometric size of the phases.

### 3.2 Thermo-Calc Analysis

Table 5 shows the results obtained at 600 °C for both steels. The reference steel has a BCC matrix (79.9%), austenite (15.3%),  $Cr_{23}C_6$  (0.4%) and Chi phase (4.4%) present in equilibrium at 600 °C. Nb addition in the steel causes the formation of NbC carbides (0.1%), and  $Cr_{23}C_6$  carbides are also present in the Nb-containing steel (0.2%), indicating that not all the carbon was stabilized by Nb addition. In the Nb-containing steel, a higher volume fraction of Chi phase is expected (5.9%), and a similar austenite percentage (16.1%) in the BCC matrix. Phases in both steels have similar chemical composition, being the Cr-rich phases Chi phase and  $Cr_{23}C_6$  carbides, and then they could be the responsible phases for the Cr-depleted regions etched after DL-EPR tests (Fig. 3). It can be also seen that partition of alloying elements are expected between equilibrium phases at 600 °C.

Despite having higher mass fraction of non-BCC matrix phases calculated in the equilibrium condition—22.3% when compared to the 20.1% of phases in the SM2Mo steel, the steel with Nb clearly has a lower content of precipitates after tempering for 2 h at 600 °C, as observed by the comparison of Fig. 3 and 4. This implies that the kinetics of tempering phase transformations for both steels were different, and this will be clarified in the next items by the experiments made with different tempering times.

### 3.3 Characterization: Different Tempering Times at 600 °C

**3.3.1 Hardness as a Function of Tempering Time.** The HRC hardness as a function of time is given in Fig. 5.

SM2Mo steel presents a typical behavior of steels during increasing tempering times: recrystallization of the martensite matrix together with the precipitation and coalescence of formed phases are expected, leading to decreasing hardness with increasing tempering times at a specific temperature. Despite the same hardness after quenching found in both steels, SM2MoNb steel had a stable behavior of hardness values during studied tempering times. The need of alloying element partition, specially Nb, probably hinders the phase transformations during tempering, allowing a stable microstructure.

**3.3.2 Degree of Sensitization as a Function of the Tempering Time.** DOS results obtained for both steels are summarized in Fig. 6, since similar DL-EPR curves (like those found in Fig. 2) have been found for all analyzed conditions. Both steels present an increasing DOS with increasing of tempering time. However, DOS found for SM2Mo steel is higher than the one found for SM2MoNb steel for all studied conditions. The need for Nb partition during tempering of the SM2MoNb steel probably makes tempering phases transformations slower, avoiding the partition of all alloying elements, creating smaller Cr- and Mo-depleted zones. This can also be seen by the analysis made with optical microscope after the DOS tests, as shown in Fig. 7(a) and (b), made at the 8 h tempering condition: in the SM2Mo steel the corrosion is generalized along the matrix and grain boundaries, while for the SM2MoNb steel the corrosion was concentrated in the grain boundaries. When Fig. 3(a) is compared with Fig. 3(b), this

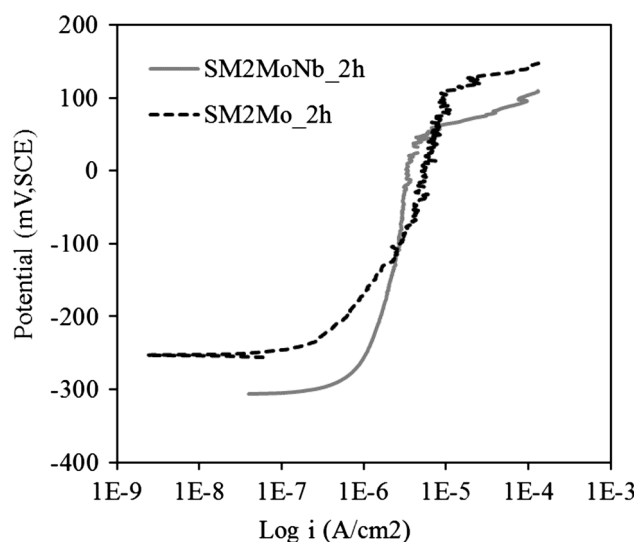


**Fig. 1** Cyclic anodic polarization curves for SM2Mo and SM2MoNb steel at 600 °C for 2 h, distilled water with 3.5% NaCl, naturally aerated

**Table 2** Tensile tests results for the SM2Mo and SM2MoNb steels

Steel	Yield strength MPa, ksi	Tensile strength MPa, ksi	Elongation, %
SM2Mo	814 ± 9 (118.0 ± 1.3)	875 ± 9 (126.9 ± 1.3)	19.2 ± 0.3
SM2MoNb	965 ± 24 (140.0 ± 3.5)	1036 ± 3 (150.3 ± 0.45)	16.5 ± 0.9

same conclusion can be made: at 2 h tempering, the steel SM2Mo has a more intense corrosion in the matrix and grain boundaries than the SM2MoNb.

**3.3.3 SEM Exams.** SEM analysis was performed using secondary electrons, in Vilella etched samples, in order to identify base microstructure and phases present. Figure 8 and 9 show both steels in the 0 and 8 h conditions. At 0 h, both steels show very similar microstructure, mainly formed by untempered martensite. However, at 8 h microstructures are quite different: the steel SM2Mo shows a high concentration of precipitated phases between the martensite needles, while in the SM2MoNb steel the precipitates seem to be concentrated at the grain boundaries and few of them could be seen in the matrix. This can be an indication that during tempering the precipitated phases in the SM2MoNb are more finely dispersed in the matrix, making their observation impossible by SEM. The finer precipitation in the SM2MoNb could be associated with the need of Nb partition, which retards the transformations during tempering, causing the observed higher hardness and smaller DOS for the SM2MoNb steel.

**Table 3 Average values and standard deviations found for Ep (mV, SCE) in 3.5% NaCl (naturally aerated) for both steels tempered at 600 °C for 2 h**

Steel	Ep, mV, SCE
SM2Mo	72 ± 35
SM2MoNb	75 ± 30

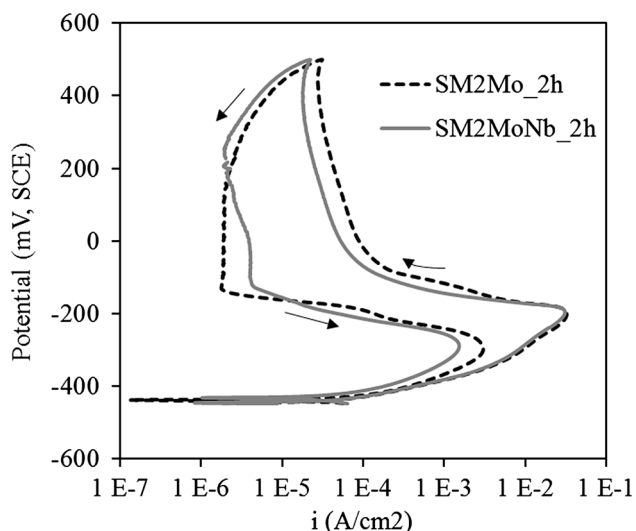


**Fig. 2** DL-EPR curves for studied steels at 600 °C for 2 h, 1M H<sub>2</sub>SO<sub>4</sub> + 0.01M KSCN electrolyte

**Table 4 Average values and standard deviations found for DOS (%), DL-EPR technique, 1M H<sub>2</sub>SO<sub>4</sub> + 0.01M KSCN for both steels tempered at 600 °C for 2 h**

	SM2Mo	SM2MoNb
DOS, 2 h tempering	6.0 ± 1.6	3.5 ± 1.7

Figure 10 shows the SM2Mo steel after 8 h tempering at 600 °C, and it is possible to see that the precipitated phase has higher corrosion resistance than the matrix, since the matrix has been uniformly etched by the Vilella reagent while the precipitated phase resisted to the etching.

**3.3.4 Non-magnetic Phase Measurement.** The measurements of non-magnetic phase have been done with a Feritscope and are shown in Fig. 11. The 0 h condition is the one with the highest amount of non-magnetic phases for both steels; this can be attributed to the presence of austenite, retained upon quenching. After tempering, the steel with Nb has always a higher percentage of non-magnetic phases present, and the hindering of the phase transformations probably caused by the need for Nb partition can be an explanation for the higher non-magnetic phase content, since a higher fraction of retained austenite will still be present in the SM2MoNb steel, as well as the presence of finer precipitation already supposed. Those assumptions are in accordance with the hardness behavior (Fig. 5) already discussed.

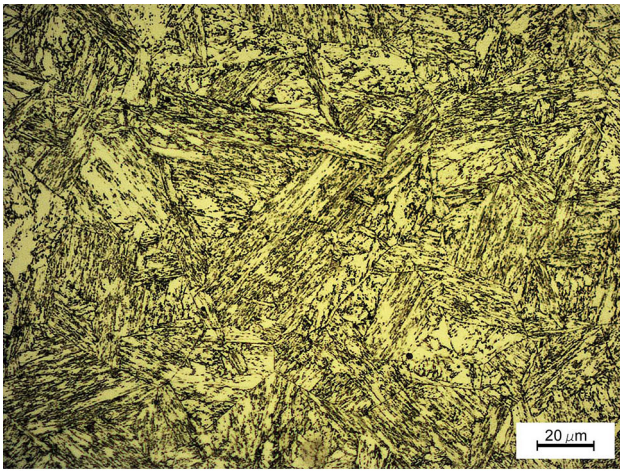
**3.3.5 X-ray Diffraction Analysis.** The diffractograms made for the steels in all the tempering conditions are shown in Fig. 12 for the SM2Mo steel and in Fig. 13 for the SM2MoNb steel. SM2Mo steel diffractogram in Fig. 12 shows that as the tempering time increases from 1 to 2 h, a peak on the left side of the highest ferrite/martensite ( $\alpha$ ) peak appears. For tempering times higher than 2 h, the presence of such peak becomes clearer. At 4 and 8 h tempering times, other peaks can be seen. According to the database, they are probably related to the presence of austenite. Even considering that Chi phase or Cr<sub>23</sub>C<sub>6</sub> carbides present some diffraction peaks closer to the ones of austenite phase (Ref 15-17), as presented in Table 5, in equilibrium conditions at 600 °C the amount of Chi phase or Cr<sub>23</sub>C<sub>6</sub> carbides is much smaller than the expected austenite fraction, and one must remember that phases with volume fractions under 5% are very unlikely to appear in XRD. Since austenite volume fractions in equilibrium lie between 15 and 16 vol.%, the peaks observed in Fig. 12 and 13 belong to austenite and ferrite phases, as indicated.

For the SM2MoNb steel, as shown in Fig. 13, the same peaks corresponding to ferrite/martensite ( $\alpha$ ) and austenite ( $\gamma$ ) can be found. However, the peak on the left of the highest intensity peak, seen clearly on the SM2Mo steels for tempering times above 2 h, is hardly seen for the SM2MoNb steel. Retained austenite formed during quenching is probably located intralath in martensite and will probably have nanometric thickness. The smaller is the size of the phase, the boarder is its diffraction peaks, making difficult their identification. With the progress of the tempering phase transformations, and considering that austenite is a stable phase in the microstructure (Table 5), the nanometric laths of retained austenite must undergo coalescence processes. If this hypothesis is valid, the need for Nb partition in SM2MoNb steel will retard the coalescence of austenite, explaining why only the diffraction peak for the (111) plane of austenite (the one with the highest intensity in ICDD cards) (Ref 16) in the SM2MoNb steel is clearly observed after tempering.

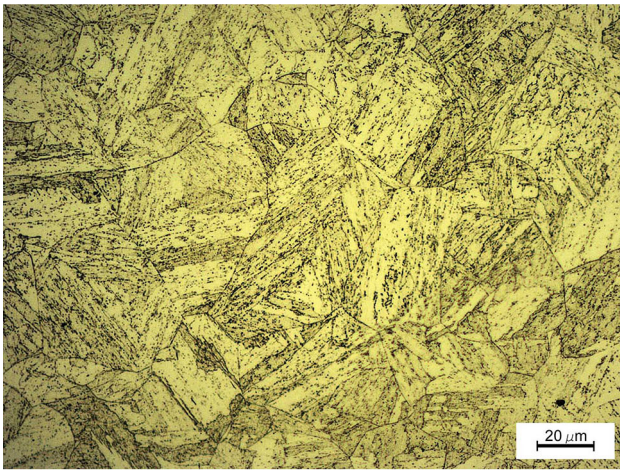
## 4. Discussion

All the analyses made as a function of time show that the addition of Nb in the 13Cr-2Mo-5Ni steels hinders the phases





(a)

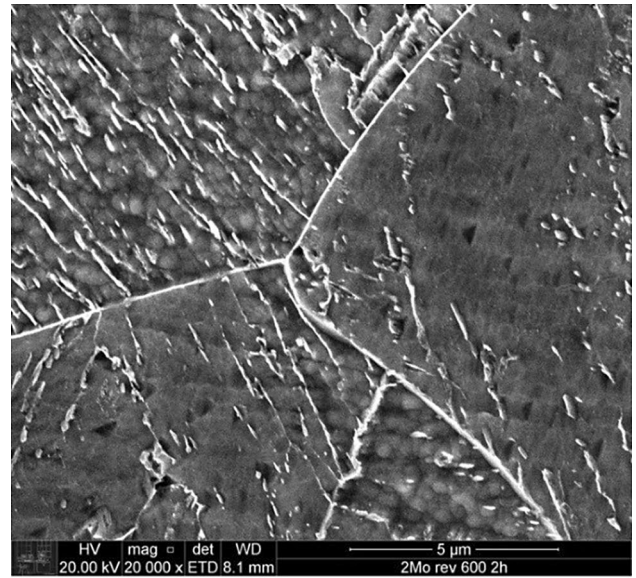


(b)

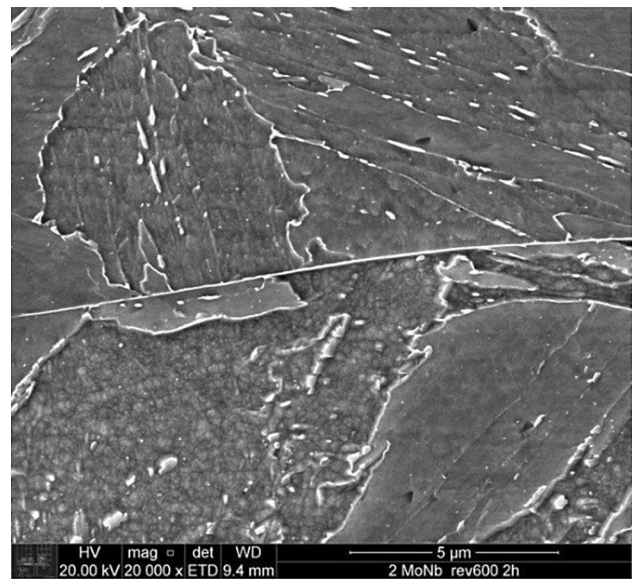
**Fig. 3** Optical micrographs after DOS tests condition 2 h tempering. (a) SM2Mo steel and (b) SM2MoNb steel

transformations that could happen during tempering, since SM2MoNb presented higher hardness than SM2Mo: the phase transformations expected during tempering (precipitation of carbides and Chi phase, expected from Thermo-Calc equilibrium simulations—Table 5, recrystallization of the martensitic matrix and a possible coalescence of the former retained austenite) may be retarded by the need of Nb partition between phases.

Such delay is also seen in the DOS tests (Fig. 6); the values found for the SM2MoNb steel are always lower when compared to the SM2Mo steel. The formation of NbC in replacement of  $Cr_{23}C_6$  is one of the factors responsible for the lower DOS values, but it is not the only one. In the SM2Mo steel, 0.4% of  $Cr_{23}C_6$  can be formed according to the Thermo-Calc, together with 4.4% Chi phase. The Chi phase is rich in chromium (around 22%) and is also responsible for the formation of poor chromium regions when precipitated and, therefore, for the increase in the DOS values. The steel with Nb has a small fraction of NbC formed (0.1%), a lower fraction of  $Cr_{23}C_6$  (0.2%) and a higher volume fraction of Chi phase (5.9%), therefore, higher DOS values would be expected. However, this is not seen in Fig. 3(a) and (b) and Fig. 7(a) and (b): SM2MoNb steel always show, for the same tempering condition, a less intense precipitation than the SM2Mo steel, despite the fact that the Thermo-Calc calculation predicts a



(a)



(b)

**Fig. 4** SEM pictures of (a) SM2Mo steel and (b) SM2MoNb steel, tempered for 2 h at 600 °C. Vilella etchant, 20,000 times magnitude, secondary electrons

more intense precipitation in the SM2MoNb steel at thermodynamic equilibrium. This is also an indicative that Nb hinders the phase transformation during tempering, or the difficult in Nb partition lead to a more finely dispersion of Cr-rich precipitates, leaving smaller regions of Cr depletion. The same is seen in SEM exams. SM2MoNb steel has always a lower amount of precipitated phases when compared to the SM2Mo steel in the same tempering condition (Fig. 4a, b, 9a, b).

The non-magnetic phase measurement, done with the Feritscope, also shows that in the SM2MoNb steel there is a hindering phase transformation effect. At 0 h, the retained austenite fraction is almost the same in both steels. At 1 h tempering, however, the steel with Nb has approximately double the amount of non-magnetic phase fraction than the SM2Mo steel. The retained austenite in the SM2Mo has transformed in ferrite, Chi phase and carbides, while in the



**Table 5** Phases present in the equilibrium and its chemical composition in SM2Mo and SM2MoNb steels at 600 °C (wt.%)

Phases	wt.%	Chemical composition, %						
		Fe	C	Cr	Ni	Mo	Nb	Si + Mn
SM2Mo at 600 °C								
Austenite	15.3	72.4	2 ppm	10.9	13.0	1.1	...	2.6
Ferrite	79.9	82.5	$7.9 \times 10^{-6}$	12.1	3.6	1.1	...	0.7
M <sub>23</sub> C <sub>6</sub>	0.4	9.3	5.1	65.4	0.3	19.9	...	0.03
Chi	4.4	57.3	...	21.9	3.3	17.5	...	...
SM2MoNb at 600 °C								
Austenite	16.1	72.2	1.9 ppm	11.1	13.1	1.1	67 ppm	2.4
Ferrite	77.7	82.2	0.1 ppm	12.5	3.7	1.1	73 ppm	0.7
NbC	0.1	54 ppm	10.4	0.2	$2.2 \times 10^{-6}$	$3.6 \times 10^{-5}$	89.4	0.4 ppm
M <sub>23</sub> C <sub>6</sub>	0.2	9.1	5.1	65.6	0.3	19.9	...	0.02
Chi	5.9	57.3	...	22.2	3.36	17.2	...	...

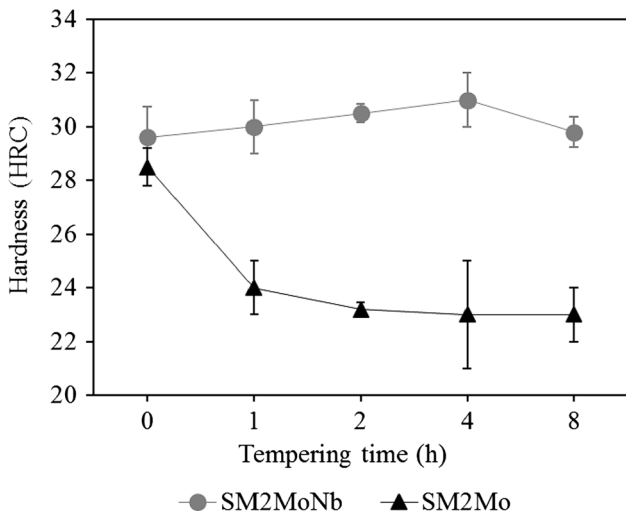


**Fig. 5** HRC hardness measurements as a function of tempering time for SM2Mo and SM2MoNb steels

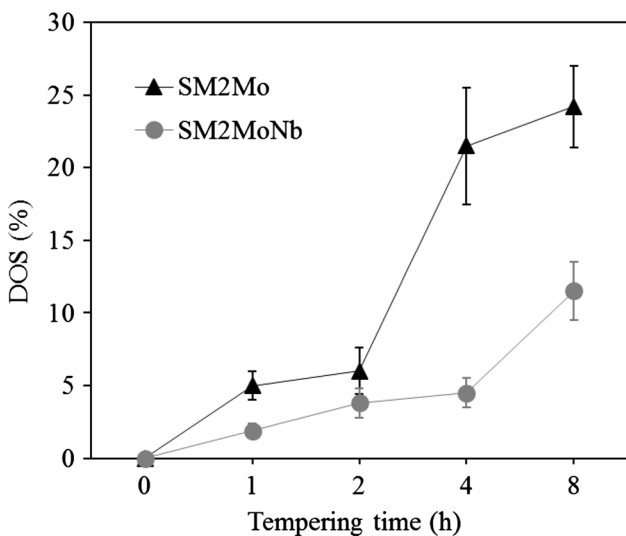
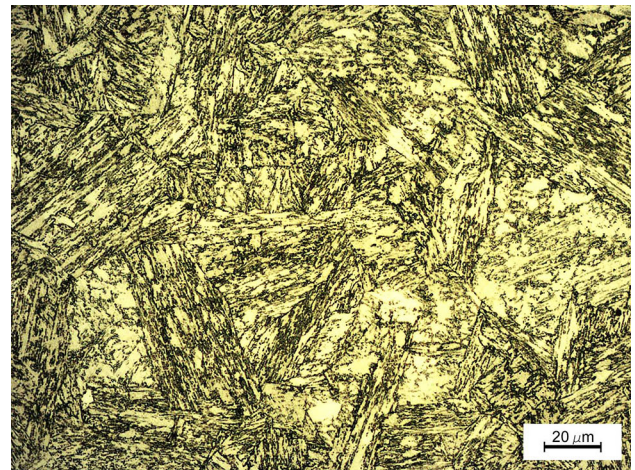
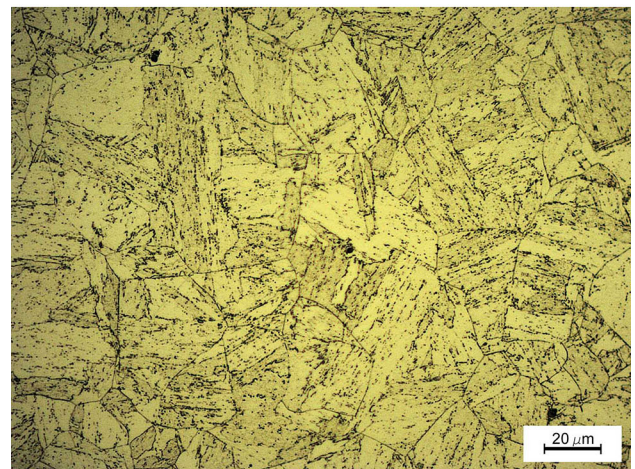


**Fig. 6** Degree of sensitization (DOS) in % as a function of tempering time for steels SM2Mo and SM2MoNb



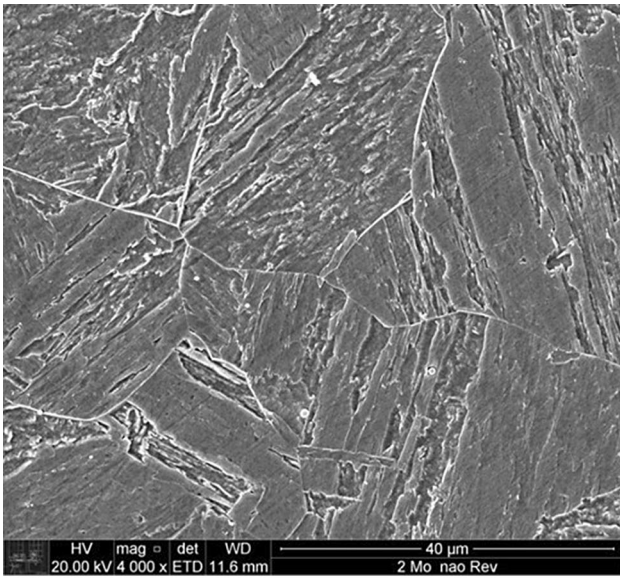
(a)



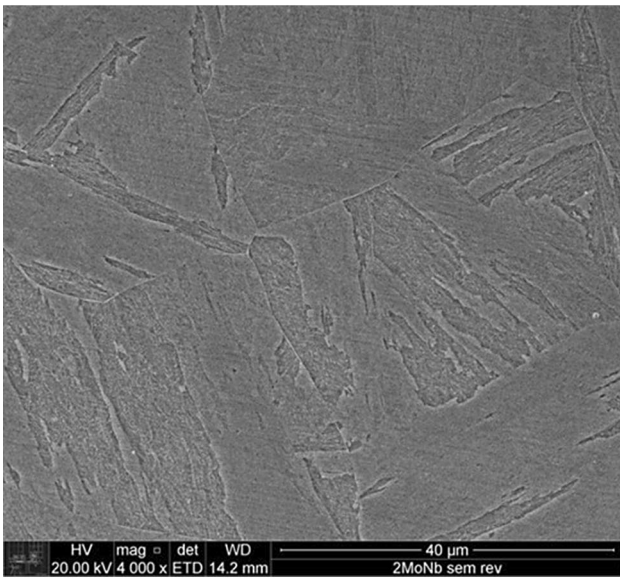
(b)

**Fig. 7** Optical micrographs after DL-EPR tests for 8 h tempering at 600 °C: (a) SM2Mo steel and (b) SM2MoNb steel

SM2MoNb steel a small amount of retained austenite has partially transformed, resulting in a higher fraction of non-magnetic phase. This can be seen in the micrographs after DOS tests: Fig. 3 reveals a more intense precipitation of Cr-rich phases (Cr<sub>23</sub>C<sub>6</sub> and Chi phase) in the SM2Mo steel than in the SM2MoNb steel.



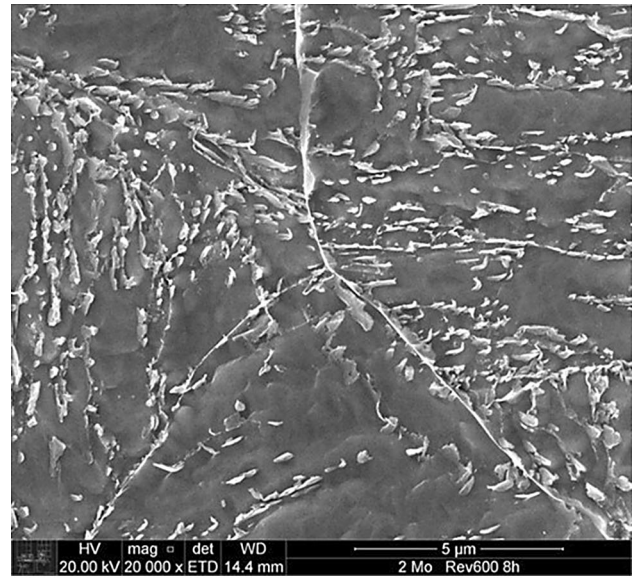
(a)



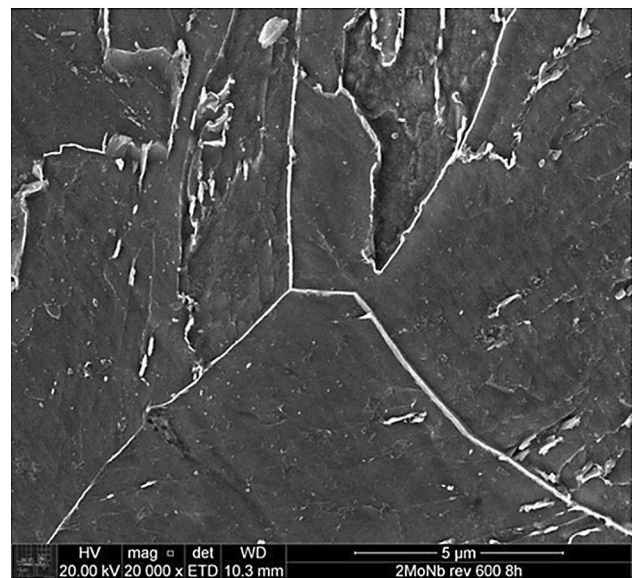
(b)

**Fig. 8** SEM pictures of (a) SM2Mo steel and (b) SM2MoNb steel, at 0 h tempering. Vilella etchant, 20,000 times magnitude, secondary electrons

Despite the high amounts of austenite, it was not possible to detect it using SEM due to the morphology of the austenite formed: according with the studies made by Ma et al. (Ref 6, 7), austenite in SMSS is in the form of films between the martensite needles, being able only to be detected by higher magnification techniques such as transmission electron microscopy (TEM). As the Cr-poor areas increase with the increase of tempering time and as the peak on the left of the XRD also become clearer in the SM2Mo steel, it is possible to conclude that retained austenite experience coalescence during tempering, and Nb partitioning is probably hindering that transformation.



(a)



(b)

**Fig. 9** SEM pictures of (a) SM2Mo steel and (b) SM2MoNb steel, at 8 h tempering. Vilella etchant, 20,000 times magnitude, secondary electrons

Nb is already known to delay the transformations that occur during tempering. In works of Pickering (Ref 18) and Irvine et al. (Ref 19), Nb in solid solution in a martensitic stainless steel with 12%Cr is related to delaying of tempering transformations. This delay in the phase transformation during tempering can be attributed to the presence of Nb as, like the other elements, it needs to be partitioned in order to allow the formation of different phases during tempering. As Nb has a big atomic radius, it delays the partitioning process, delaying the phase transformation start and progress during tempering.



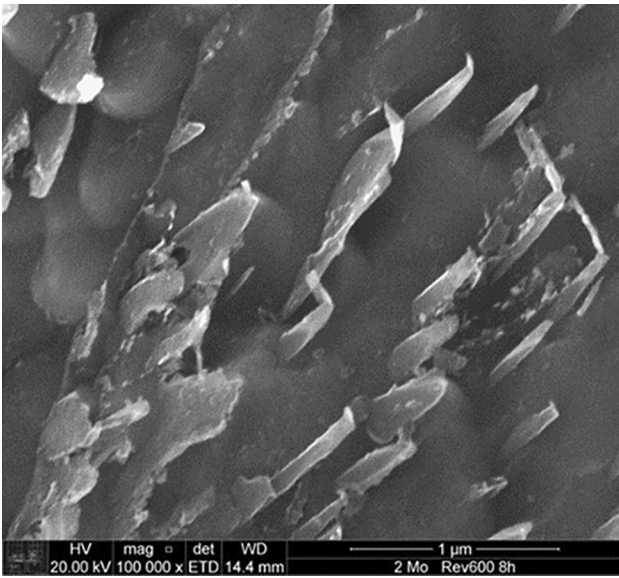


**Fig. 10** SEM pictures of SM2Mo steel at 8 h tempering. Vilella etchant, 100,000 times magnification, secondary electrons

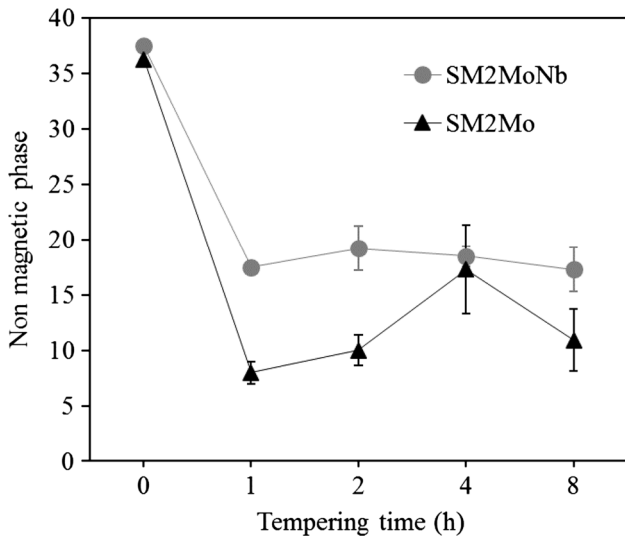


**Fig. 11** Non-magnetic phase (%) as a function of the tempering time at 600 °C for steel SM2Mo and SM2MoNb

## 5. Conclusions

1. Nb addition in the 13Cr-5Ni-2Mo steel tempered for 2 h at 600 °C improves the yield and tensile strength without compromising the elongation and the pitting corrosion resistance. The steel is also less prone to sensitization as the DOS obtained for the SM2MoNb steel is half of the SM2Mo one.
2. Both steels can be classified as Grade 110 by the ISO 13680:2010. However, the steel with Nb is in the upper limit of the specification, which suggests the possibility of obtaining a higher grade, not specified in the standard. Regarding hardness, the steels also comply with the standard.

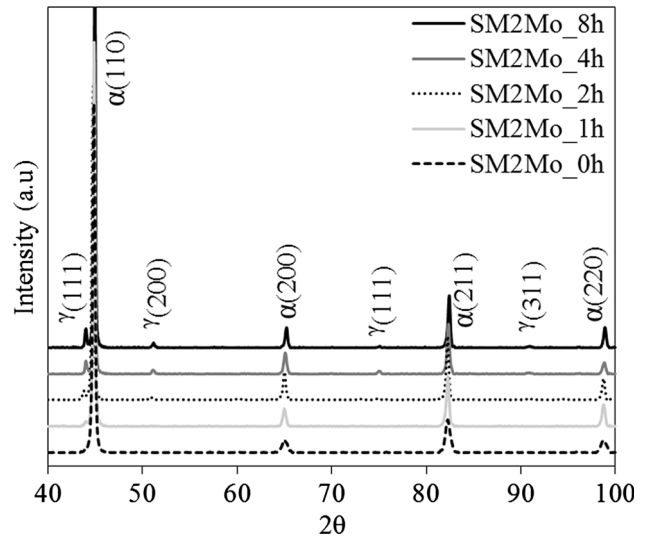


**Fig. 12** X-ray diffractograms for different tempering times for the SM2Mo steel. The peaks indicated by  $\alpha$  refer to a ferrite/martensite microstructure

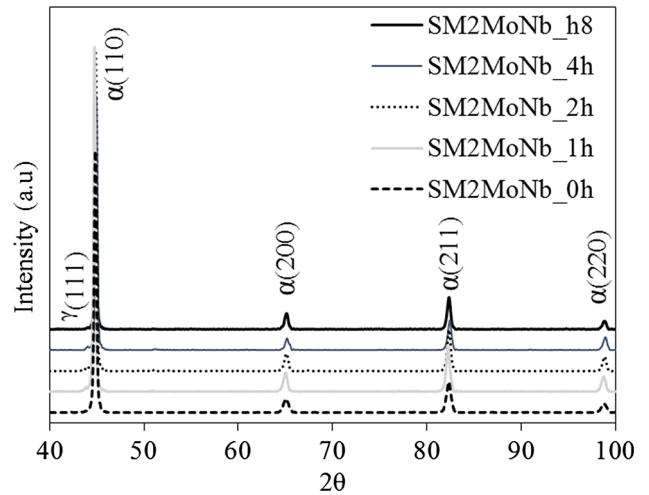


**Fig. 13** X-ray diffractograms for different tempering times for the SM2MoNb steel. The peaks indicated by  $\alpha$  refer to a ferrite/martensite microstructure

3. Higher mechanical resistance of the SM2MoNb steel is also shown by the hardness measurements: the average values obtained in the SM2MoNb steel are always higher than the ones obtained for the SM2Mo steel.
4. Steels present similar behavior during tempering treatment, but delayed in time, and this is attributed to partitioning of the elements, especially Nb, necessary to allow phase transformation.
5. DOS is always smaller for the SM2MoNb steel, independently of the tempering time used. Its evolution is directly related to the phase transformation that occurs during tempering. The presence of Nb in the 13Cr-2Mo-5Ni steels may lead to a finer distribution of austenite and Chi phases, creating smaller Cr-depleted zones in the SM2MoNb steel.



## References

1. K. Kondo, M. Ueda, K. Ogawa, H. Amaya, H. Hirata, H. Takabe, and Y. Miyazaki. Alloy design of super 13Cr – Development of super 13Cr martensitic stainless steel for line pipe-1. *Supermartensitic Stainless Steels 99*, Belgium Welding Institute, Belgium, 1999
2. P. Toussaint and J.J. Dufrane. *Advances in the Making and Base Material Properties of Super Martensitic Stainless Steels (SMSS)*. Supermartensitics 2002, KCI Publishing BV, Belgium, 2002
3. C. Jochum, H. Heuser, and R. Sölch. *Properties of Matching Filler Metals for Supermartensitic Pipelines*. Supermartensitics 2002, KCI Publishing BV, Belgium, 2002
4. T.G. Gooch, P. Wollin, and A.G. Haynes. Welding Metallurgy of Low Carbon 13% Chromium Martensitic Steels, *Supermartensitic Stainl. Steels*, 99:S99-22 (Belgium), 1999, pp. 188–195
5. P.A. Schweitzer. *Fundamentals of Metallic Corrosion: Atmospheric and Media Corrosion of Metals*, CRC Press – Taylor & Francis Group, 2nd ed, US, 2007, p. 110
6. X. Ma, Z. Cheng, W. Lijung, L. Chunming, S. Subramanian, and M.P. Oliveira. Role of Nb in 13Cr supermartensitic stainless steel. *10th Brazilian Stainless Steel Conference*, Rio de Janeiro, Brazil, 2010
7. X. Ma, L.J. Wang, C.M. Liu, and S.V. Subramanian, Role of Nb in Low Interstitial 13Cr Super Martensitic Stainless Steel, *Mater. Sci. Eng A*, 2011, **528**, p 6812–6818
8. X. Ma, L. Wang, S.V. Subramanian, and L. Chunming, Studies on Nb Microalloying of 13Cr Super Martensitic Stainless Steel, *Metall. Mater. Trans. A*, 2012, **43A**, p 4475–4486
9. X. Ma, L. Wang, M. P. Oliveira, L. Chinming, and V. Subramanian. Structure-property studies on Nb microalloyed 13%Cr super martensitic stainless steel. *Baosteel Conference – BAC 2013*, Shanghai, China, 2013
10. D. Zou, Y. Han, W. Zhang, and X. Fang, Influence of Tempering Process on Mechanical Properties of 00Cr13Ni4Mo Supermartensitic Stainless Steel, *J Iron Steel Res Int*, 2010, **17–8**, p 50–54
11. C. Passanante, M. P. Oliveira, J. W. Calderón-Hernández, D. Hincapié-Ladino, and N. Alonso-Falleiros. Influência da Porcentagem da Fase Ferrita Delta na Resistência à Corrosão por Pite de um Aço Inoxidável Supermartensítico. *69º Congresso Anual da ABM Internacional*, Brazil, 2014
12. Standard Test Methods for Rockwell Hardness of Metallic Materials. E18, ASTM Standards, 2014
13. Standard Test Methods and Definitions for Mechanical Testing of Steel Products. A370, ASTM standards, 2010
14. Petroleum and natural gas industries – Corrosion-resistant alloy seamless tubes for use as casing, tubing and coupling stock – Technical delivery conditions. 13680, ISO standards, 2010
15. The International Centre for Diffraction Data (ICDD). PDF card no. 00-006-0674, 2010
16. The International Centre for Diffraction Data (ICDD). PDF card no. 00-033-0397, 2010
17. The International Centre for Diffraction Data (ICDD). PDF card no. 00-035-0783, 2014
18. F.B. Pickering. Physical metallurgical development of stainless steels. In *Stainless Steels'84, The Institute of Metals*, London, 1985, p. 2–28
19. K.J. Irvine, J. Crowe, and F.B. Pickering. The physical metallurgy of 12%Cr steels. In *The Metallurgical Evolution of Stainless Steels, American Society for Metals (ASM)*, US, 1979, p. 43–69